Hindawi
International Journal of Distributed Sensor Networks
Volume 2023, Article ID 6671730, 15 pages
https://doi.org/10.1155/2023/6671730

Research Article

Weak Fault Feature Extraction for Rolling Element Bearing Based on a Two-Stage Method

LianHui Jia,[1,2] LiJie Jiang,[2] YongLiang Wen,[2] and Hongchao Wang[3]

[1]*School of Mechanical Science and Engineering, Huazhong University of Science and Technology, Wuhan, Hubei 430074, China*
[2]*China Railway Engineering Equipment Group Co., Ltd, No. 99, 6th Avenue National Economic & Technical Development Zone, Zhengzhou 450016, China*
[3]*Mechanical and Electrical Engineering Institute, Zhengzhou University of Light Industry, 5 Dongfeng Road, Zhengzhou 450002, China*

Correspondence should be addressed to Hongchao Wang; hongchao1983@126.com

Received 6 February 2023; Revised 25 April 2023; Accepted 25 May 2023; Published 21 June 2023

Academic Editor: Diego Alexander Tibaduiza

Timely and effective feature extraction is the key for fault diagnosis of rolling element bearing (REB). However, fault feature extraction will become very difficult in the early weak fault stage of REB due to the interference of strong background noise. To solve the above difficulty, a two-stage feature extraction method for early weak fault of REB is proposed, which mainly combines feature mode decomposition (FMD) with a blind deconvolution (BD) method. Firstly, based on the impulsiveness and cyclostationary characteristics of the vibration signal of faulty REB, FMD is used to decompose the complex original vibration signal into several modes containing single component. Subsequently, the sparse index (SI) is calculated for each mode, and the mode containing sensitive fault feature is selected for further analysis. Subsequently, apply the deconvolution method on the selected mode for further enhancing the impulsive characteristic. At last, traditional envelope spectrum (ES) analysis is applied on the filtered signal, and satisfactory fault features are extracted. Effectiveness and advantages of the proposed method are verified through experimental and engineering signals of REBs.

1. Introduction

REBs are commonly utilized in various industrial applications, such as helicopters, high-speed trains, and wind turbines [1]. As the most commonly used component in rotating machinery, REB is also one of the most prone to failure components. Research on prognosis of REBs has becoming one hot area in recent decades. Effective fault feature extraction could provide powerful support for timely and correct fault diagnosis of REB. Significant progress has been made in the area of feature extraction based on vibration signal processing methods: from the initial FFT [2], ES analysis [3], wavelet transform (WT) [4], empirical mode decomposition (EMD) [5], variational mode decomposition (VMD) [6], spectral kurtosis (SK) [7] and its improved methods [8–11], minimum entropy deconvolution (MED) [12] and its improved methods [13–16], cyclostationarity theory with its related researches [17–19], to the later sparse decomposition [20–24] and denoising method based on deep learning [25–30]. However, the performance of some of the above methods is more or less insufficient when the characteristic signal of faulty REB is disturbed by strong background noise, especially in the early weak fault stage of REB, which will be verified in the comparison section.

It is well known that the vibration signal of faulty REB often presents periodic shock characteristics. ES analysis is a traditional and effective method for extracting the fault features of REB. However, it often fails to achieve satisfactory results by applying full-band ES on the original signal of faulty REB directly, and it is an important research direction to study how to select a frequency band containing a large number of shock components and then perform ES analysis on the selected frequency band, that is, the resonance demodulation technology (RDT). The above-mentioned SK analysis method is the milestone representative of RDT. Unfortunately, as proved by McDonald et al. [13], SK is

sensitive to the instantaneous shock and could not reflect the continuous periodic shock characteristics of the vibration signal of faulty REB effectively, which often leads to misjudgment. Although the improved methods of SK have solved the above-mentioned shortcoming of SK to some extent, as stated in reference [31], the selected frequency band in the above improved methods of SK might not be the optimal frequency band due to the influence of strong background noise and the complexity of signal components. In addition, the periodic shock characteristic components might be divided into two adjacent frequency bands, resulting in the loss of useful information. Furthermore, the noise and interference components in the selected frequency band might also be enhanced by RDT, which further hinders its wonderful performance. BD is another effective method to enhance the impact characteristic signal of REB and eliminate the effect of signal acquisition path on signal attenuation, which filters the original signal by finding an optimal inverse finite impulse response (FIR) filter to eliminate noise and interference components. Selection of the optimal filter parameters is achieved by minimizing or maximizing a specific index of the filtered signal. The classical BD method, also well known as MED, maximizing the kurtosis of the filtered signal is used in fault diagnosis of rotating machinery successfully [12]. Aiming at the sensitivity of the kurtosis index to additional shock interference, the OMED [32] method is proposed, which solves the above shortcomings of MED to a certain extent. The shock index can describe the cyclic shock characteristics of the signal of faulty REB effectively and is used in the BD method [33]. Besides, kinds of BD methods based on other indicators have been proposed one after another and have been widely used in the fault diagnosis of REB [34–37]. The above BD methods do not consider the prior information of faulty REB into BD, and some BD researches try to apply prior information to BD, among which the fault characteristic frequency of faulty REB is the most commonly used prior information. Based on the prior fault characteristic frequency, a BD method based on maximum correlation kurtosis, namely, MCKD method, is proposed [13]. Subsequently, kinds of BD methods based on the prior information such as defined target vector [38] and cyclostationarity [39, 40] have been arising. Inspired by the above BD researches' idea based on prior information, the fault characteristic period of faulty REB, this paper used a BD method based on an index describing the noise intensity of periodic cyclostationary signal. The used BD method not only could demodulate one or more resonance frequency bands excited by periodic shock components adaptively but also can eliminate the fault-irrelevant frequency components in the resonance frequency band effectively.

Due to the complexity and diversity of the original signal components of faulty REB, although the repetitive impacts could be enhanced by the used BD method, the intrinsic characteristic of the other components might also be enhanced simultaneously. Adaptive nonstationary signal processing methods such as WT, EMD, and VMD can decompose nonstationary vibration signals into a series of single-component signals and perform BD methods on the decomposed single-component signal that could solve the above problems to a certain extent. However, the selection of the WT base function has great chance on the decomposition result, and it is necessary to know the prior knowledge of the signal to be analyzed in advance to establish the optimal wavelet base in order to obtain satisfactory decomposition effect. EMD has the problem of modal aliasing. Although the subsequent improved methods of EMD [41–43] can overcome the mode aliasing problem effectively, they often have the disadvantage of large amount of calculation. VMD needs to determine the optimal mode decomposition order in advance, which is difficult to be achieved in most engineering applications. As a new no-stationary time-frequency method, FMD [44] takes the impulsiveness and periodicity of fault signal into consideration simultaneously and could remove the redundant and mixing modes adaptively in the decomposition process. So FMD is used in the paper as an alternative to the above traditional TF analysis methods and is used as preprocessing method for the used BD method.

Based on the above stated, a two-stage feature method for early weak fault detection of REB is proposed in the paper, and its main steps are as follows: firstly, the original fault signal of REB containing complex and multicomponent is decomposed by FMD, and a series of modal signals with a single component is obtained. Subsequently, the sparse index (SI) is used to measure the amount of repetitive impacts being contained in each mode. Thirdly, a BD method is applied on the selected mode with biggest value of SI for further fault feature enhancement. At last, ES is applied on the filtered signal of the used BD algorithm, and satisfactory fault features are extracted. The main contributions of this paper are as follows:

(1) SI is used to reflect the amount of repetitive impacts buried in the vibration signal of faulty REB, which is much more reliable than the other index such as kurtosis and the other indexes

(2) The BD method not only could demodulate one or more resonance frequency bands excited by periodic shock components adaptively but also can eliminate the fault-irrelevant frequency components in the resonance frequency band effectively

(3) FMD is used as preprocessing method for the BD method, and the combined method has advantages over the other related methods

The remains of the paper are organized as follows: Section 2 is dedicated to the BD method. Flow chart of the proposed method and its details are given in Section 3. Section 4 and Section 5 are the experiment and engineering verifications, respectively. Comparison is carried out in Section 6, and conclusions are obtained in Section 7 at last.

2. The BD Method

The filtering process of BD could be represented by

$$x = s * f, \tag{1}$$

where s is the observed signal and its length is represented by N, f represents an optimal FIR to be solved with size of L, and $*$ is the convolution operation. x represents the filtered signal. The matrix form of equation (1) could be written as

$$x = S_0^T f, \tag{2}$$

in which

$$f = \begin{bmatrix} f_1 \\ f_2 \\ \vdots \\ f_{L-1} \\ f_L \end{bmatrix}, \quad S_0 = \begin{bmatrix} s_1 & s_2 & s_3 & \cdots & s_N \\ 0 & s_1 & s_2 & \cdots & s_{N-1} \\ 0 & 0 & s_1 & \cdots & s_{N-2} \\ \vdots & \vdots & \vdots & \ddots & \vdots \\ 0 & 0 & \cdots & \cdots & s_{N-L+1} \end{bmatrix}. \tag{3}$$

The solution of BD is to solve the gradient of the objective function J to filter f. Maximizing (minimizing) the objective function J of the filtered signal x usually requires solving the following equation:

$$\frac{\partial J(x)}{\partial f} = \frac{\partial J(s * f)}{\partial f} = 0. \tag{4}$$

The periodic noise amplitude ratio (PNAR) [45] is used as the index measuring the level of noise contained in the original vibration signal of faulty REB, whose definition is as follows:

$$\mathrm{PNAR}(x, t_{\mathrm{noise}}) = \frac{\sqrt{N}}{M} \frac{t_{\mathrm{noise}} \cdot \mathrm{abs}(x)}{\|x\|_2}, \tag{5}$$

where $\mathrm{abs}(x)$ denotes the absolute value of filtered signal x, the number of the defined noise points is represented by M, and $\|\cdot\|_2$ is the Euclidean norm. t_{noise} is expressed as

$$t_{\mathrm{noise}} = [0, \cdots, 0, 1, \cdots, 1, 0, \cdots, 0, 1, \cdots, 1, 0, \cdots], \tag{6}$$

where t_{noise} has the same length as x and it marks the positions of the defined noise points in the filtered signal: The noise points are noted by 1, and the repetitive impact points are noted by 0.

It could be observed based on equation (5) that PNAR is the ratio of the average amplitude of marked noise points to the RMS value of the filtered signal. If there exists noise in the signal, the value of PNAR will increase to a certain degree, which means that the smaller value of PNAR, the better filtering effect of BD result. As for the noised repetitive impulse characteristic components of faulty REB, though the internal between adjacent impulse positions could not be equal to the fault period T strictly, the impulsive components with higher amplitudes are not marked by t_{noise}. t_{noise} could be calculated by

$$\rho = \frac{N}{T}, \tag{7}$$

where N is the continuous points in one fault period and T is the fault period, which could be calculated by the prior known information such as rotating speed and the parameters of the diagnosed REB. The same as reference [45], the value of ρ is set as 0.6.

The basic theory of the used BD is as follows:

$$\min_f \mathrm{PNAR}(x, t_{\mathrm{noise}}) = \min_f \frac{\sqrt{N}}{M} \frac{t_{\mathrm{noise}} \cdot \mathrm{abs}(x)}{\|x\|_2}. \tag{8}$$

The solution of gradient from PNAR to filter f is as follows:

$$g = \frac{\partial \mathrm{PNAR}(x, t_{\mathrm{noise}})}{\partial f} = \frac{\partial \mathrm{PNAR}(x, t_{\mathrm{noise}})}{\partial x} \cdot \frac{\partial x}{\partial f}. \tag{9}$$

The following equation could be obtained based on equation (2) and equation (9):

$$\frac{\partial x}{\partial f} = \frac{\partial (s^* f)}{\partial f} = S_0. \tag{10}$$

The solution of the PNAR's gradient could use the backward automatic differentiation algorithm [46].

The second step is to update filter f by using the Adam algorithm, and the first-order estimation and second-order momentum estimation of the gradient g_t are calculated by the Adam algorithm, in which g_t represents the corresponding value at the ith iteration.

$$\begin{aligned} m_t &= \beta_1 \cdot m_{t-1} + (1 - \beta_1) \cdot g_t, \\ v_t &= \beta_2 \cdot v_{t-1} + (1 - \beta_2) \cdot g_t \odot g_t, \\ m_0 &= 1, \\ v_0 &= 0, \end{aligned} \tag{11}$$

where $\odot$ represents the Hadamard product operation, β_1 and β_2 represent the first- and second-order momentum attenuation coefficients, respectively, and their values are set as 0.9 and 0.99 the same as reference [45].

The following equations are used to calculate $\hat{m}_t$ and $\hat{v}_t$:

$$\begin{aligned} \hat{m}_t &= \frac{m_t}{1 - \beta_1^t}, \\ \hat{v}_t &= \frac{v_t}{1 - \beta_2^t}, \end{aligned} \tag{12}$$

Update filter f at the ith step using the following equation:

$$f_t = f_{t-1} - \frac{\alpha}{\sqrt{\hat{v}_t} + \varepsilon} \cdot \hat{m}_t, \tag{13}$$

where ε is set as 10^{-8} the same as reference [45].

The detailed calculation processes of the BD method are presented in Algorithm 1.

3. Flow Chart of the Proposed Method

Flow chart of the proposed method is given in Figure 1, and the details of each step are as follows.

Step 1. Collect the vibration signal of faulty REB and input it into the calculation model of FMD (details of FMD could be referred to reference ([34]).

Step 2. The SIs of each mode obtained by FMD in Step 1 are calculated.

Step 3. The mode obtained in Step 1 with the biggest value of SI is selected for further analysis due to reason that it contains the maximum amount of repetitive impact characteristic components.

Step 4. Calculate the fault period of the diagnosed faulty type, and input it with the selected mode into the BD calculation model simultaneously.

Step 5. Apply ES analysis on the output signal obtained in Step 4, and the satisfactory fault features are extracted.

It should be noted that among the series of modes obtained in the first step, the mode containing the largest amount of repetitive impact components is often selected according to a certain index for further analysis. Among them, the kurtosis index is a commonly used classical index, but it has the disadvantage of being sensitive to additional shock components. The other subsequent index such as negative entropy [34] has the defect being sensitive to random white noise. To solve the above stated problem, the SI is used for sensitive mode selection in Step 2. The SI index has stronger noise robustness than other impact component metrics. The calculation expression of SI is shown in equation (14), in which $\|\cdot\|_1$ represents the l_1 norm, the squared envelope analysis result of the analyzed signal is represented by SE, SE^r represents sorting SE in ascending order, i.e., $\mathrm{SE}^r[1] \le \mathrm{SE}^r[2] \le \cdots \mathrm{SE}^r[N]$, and N is the number of decomposition modes. The calculation formula of SE is shown in equation (15), in which $\bar{s}$ is the analytical signal of s, $H(\cdot)$ represents the Hilbert transform, and $j^2 = -1$.

$$\mathrm{GI} = 1\text{-}2\sum_{p=1}^{N} \frac{\mathrm{SE}^r[p]}{\|\mathrm{SE}\|_1}\left(\frac{N-p+0.5}{N}\right), \tag{14}$$

$$\mathrm{SE} = |\bar{s}|^2 = |s + j \times H(s)|^2. \tag{15}$$

To verify the robustness of SI to transient shock and its reliability in measuring the periodic shock of faulty REB's vibration signal, five kinds of signals shown in equation (16) are used: Sig1 is the time-domain addition of the sinusoidal signals, Sig2 is the random noise, Sig3 is the random noise with one single shock, Sig4 is the random noise with three shocks, and Sig5 is the random noise with continuous shocks, and their corresponding time-domain waveforms are given in Figure 2(a). The four kinds of indexes (SI, Hoyer measure [47], L2/L1 [9] norm, and kurtosis) measuring the impact characteristics of the five kinds of signals are calculated, respectively, and their normalized values are shown in Figure 2(b): It could be seen that SI increases with a gradual increasing trend with the increase of impulse components through comparison. However, the other three indicators do not have the characteristic the same as GI.

$$\begin{cases} \mathrm{Sig1} = \sin\left(\dfrac{2\pi}{100}^{*} t\right) + 3\sin\left(\dfrac{2\pi^{*}}{10} t\right), \quad t = 1:1000, \\ \mathrm{Sig2} = 0.25\mathrm{randn}(\mathrm{Sig1}), \\ \mathrm{Sig3} = \mathrm{Sig2}\,; \mathrm{Sig}(700) = 8, \\ \mathrm{Sig4} = \mathrm{Sig2}\,; \mathrm{Sig}(340:233:\mathrm{end}) = 8, \\ \mathrm{Sig5} = \mathrm{Sig2}\,; \mathrm{Sig}(28:100:\mathrm{end}) = 10. \end{cases} \tag{16}$$

4. Experiment Verification

The conventional failure experiments of REB are often simulated by processing faults on the components (inner race, outer race, rolling element, or cage) of REB using EDM technology, and the fault features are often obvious, which could be extracted effectively by applying ES analysis on the original faulty signal directly, so the early weak fault of REB could not be simulated by conventional failure experiments. This experiment is more convincing to verify the effectiveness of the proposed method by using the data collected from the early failure stage of the REB accelerated fatigue life experiment. The actual picture of the test bench is shown in Figure 3(a). The so-called accelerated fatigue test is to apply additional load to the test REB to accelerate its fatigue damage rate without affecting the damage mechanism of the REB. Figure 3(b) shows the schematic diagram of the additional load loading on the experimental REB, and Figure 3(c) shows the schematic diagram of the sensor installation. The experimental data of one of the bearings is selected for analysis, and the parameters and the fault characteristic frequencies of the selected test rolling bearing are shown in Tables 1 and 2, respectively. In Table 2, f_r is the rotating frequency of the rolling bearing, f_c is the fault characteristic frequency of the rolling bearing cage, and f_b, f_i, and f_o are the fault characteristic frequencies of rolling bearing's rolling element, inner race, and outer race. One group of 20480 points is collected per minute with sampling rate 25.6 kHz. Finally, the selected REB is disassembled, and it is found that fault arises on the inner race of the selected REB. The kurtosis and amplitude indicators of the selected bearing's vibration data throughout

Input: The measured vibration signal s, the fault period T, noise ratio ρ, the iteration number N.
Initialize filter as f_0 randomly.
For $t = 1, 2, \cdots, N$, **do**
Calculate the filtered signal x: $x = s^* f_{t-1}$.
Compute the PNAR of the filtered signal x.
Compute the gradients g_t by backward automatic differentiation.
Determine the filter f_t for the next iteration via Adam.
End
Output: The filtered signal x.

Algorithm 1: The detailed calculation processes of the BD method.

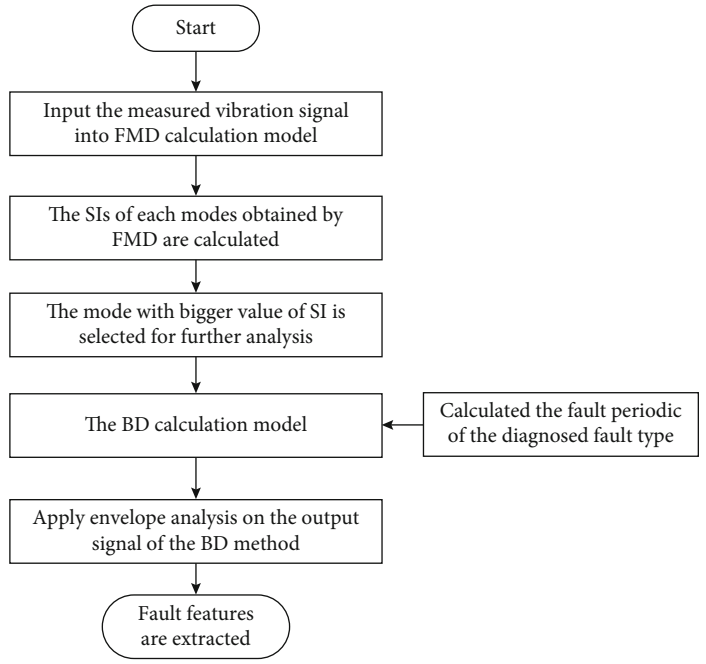

Figure 1: Flow chart of the proposed method.

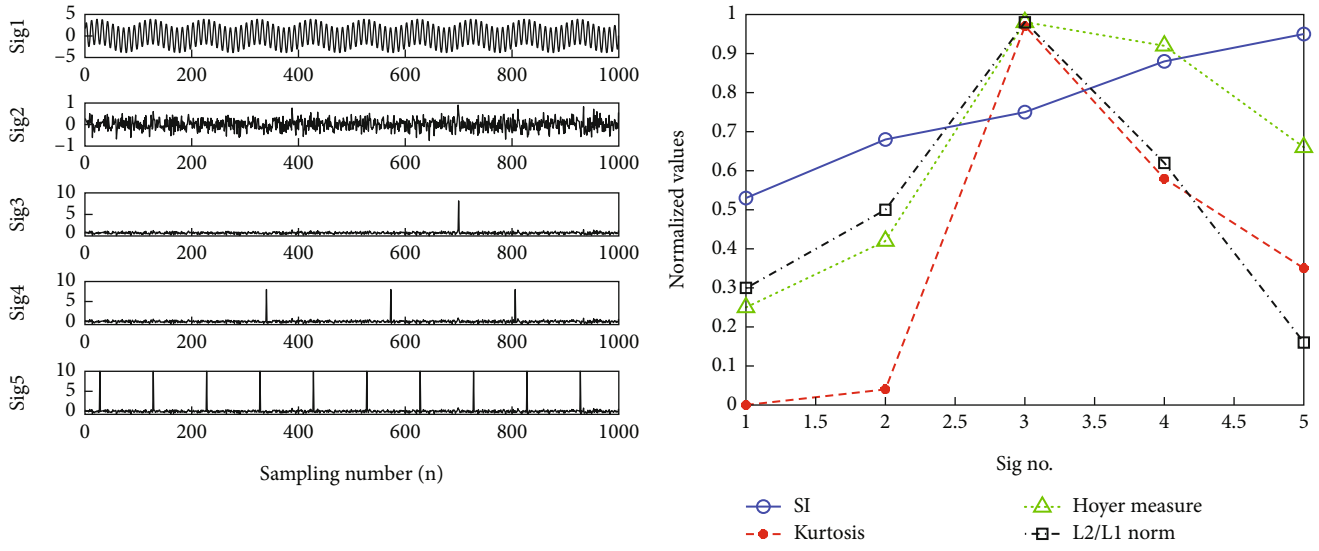

(a) Five signals

(b) Four indexes corresponding to the five signals as shown in (a)

Figure 2: Five signals with their four indexes.

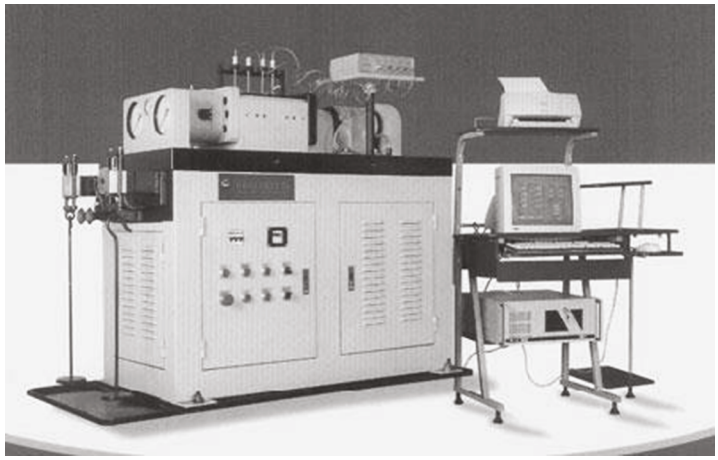

(a) Accelerated bearing life tester, ABLT-1A

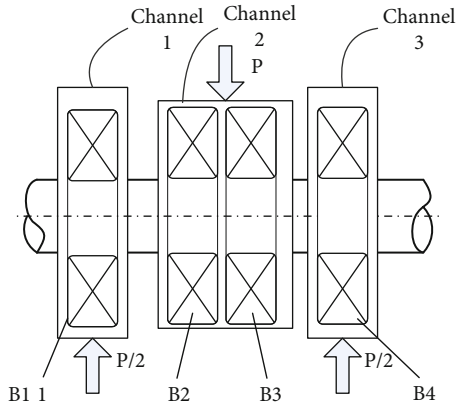

(b) Sketch of load

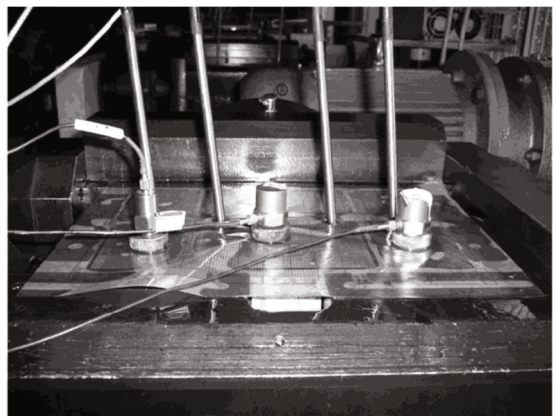

(c) Location of sensors

Figure 3: Accelerated life test of rolling element bearing.

Table 1: The parameters of the test rolling bearing.

Type	Ball number	Ball diameter (mm)	Pitch diameter (mm)	Contact angle	Motor speed (rpm)	Load (kN)
6307	8	13.494	58.5	0	3000	12.744

Table 2: The fault characteristic frequencies of the test rolling bearing.

f_r	f_c	f_b	f_i	f_o
50 Hz	19 Hz	102 Hz	246 Hz	153 Hz

its life cycle are shown in Figures 4(a) and 4(b), respectively. It could be seen that the kurtosis and amplitude indexes of the REB's life cycle data do not change abruptly before the 2297th minute, so the data collected at the 2297th minute can be regarded as the early weak stage of the selected REB, and its time-domain waveform is presented in Figure 4(c). Apply ES analysis on the original weak fault signal, and the corresponding result is given in Figure 4(d), based on which the distribution of spectral lines is disorganized, and the fault characteristic frequency of the selected bearing could not be extracted effectively.

Figure 5 gives the filtered results by applying the BD method on the original signal as shown in Figure 4(c) directly. It could be observed that the impulse characteristics are enhanced evidently compared with the original signal. The modulation phenomenon could be observed based on FFT spectrum of the filtered signal, and the inner race fault characteristic frequency (245 Hz) could be extracted by the ES of the filtered signal. However, the harmonics of the inner race fault characteristic frequency could not be extracted.

Apply the proposed method on the original experiment signal, and Figure 6(a) shows the main two decomposed modes (there are six modes obtained) by applying FMD on the original experiment signal. Then, the SI of the six modes is calculated, respectively, and the mode with bigger SI is selected for further BD analysis. The ESs of the two main obtained modes are shown in Figure 6(b), based on which the strong separation ability of FMD is further verified: The first mode mainly contains the rotating frequency components and its harmonics, and the second mode containing

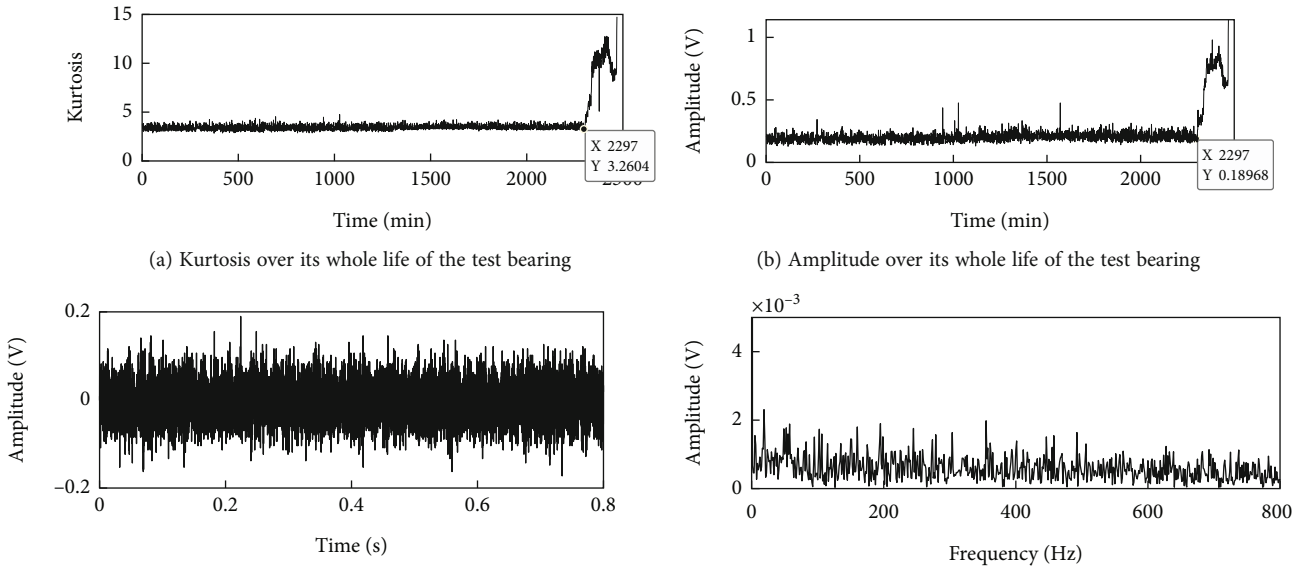

(a) Kurtosis over its whole life of the test bearing

(b) Amplitude over its whole life of the test bearing

(c) Time-domain waveform of the early weak fault signal of the selected bearing

(d) Envelope spectral analysis result of the signal as shown in (c)

Figure 4: Early weak fault signal of experimental rolling element bearing.

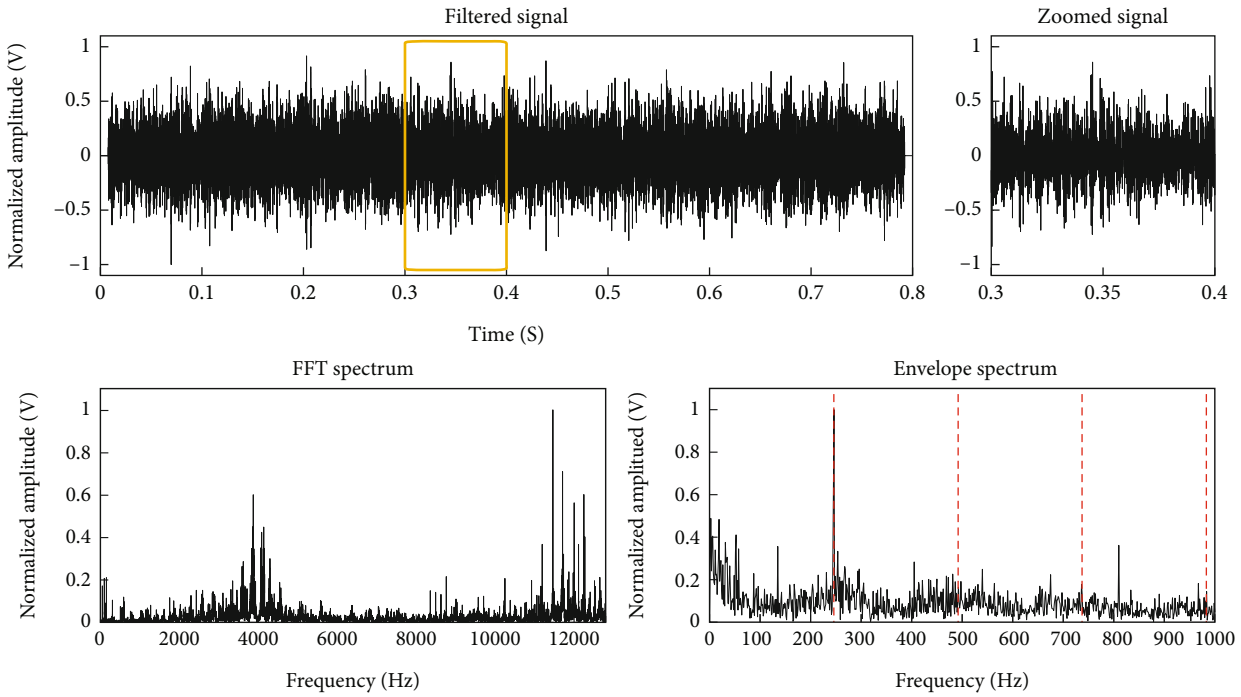

Figure 5: Early weak fault signal of experimental rolling element bearing handled by the proposed BD method directly.

impulse characteristic components is still influenced by noise, because the inner race fault characteristic frequency could not be identified. Subsequently, the impulse characteristic of the second mode is enhanced by the BD method, and the results are presented in Figure 7 based on which the inner race fault characteristic frequency (245 Hz) with its harmonics of the selected REB is extracted successfully, and effectiveness of the proposed method is verified. Besides, whether compared with the original signal shown in Figure 4(c) or to the BD filtered signal shown in Figure 5, the impulse feature enhancement effect of the proposed method is the best.

5. Engineering Verification

The engineering inspected object is the raw material grinding equipment of a cement plant. Schematic diagram of the unit structure is shown in Figure 8: The output speed of

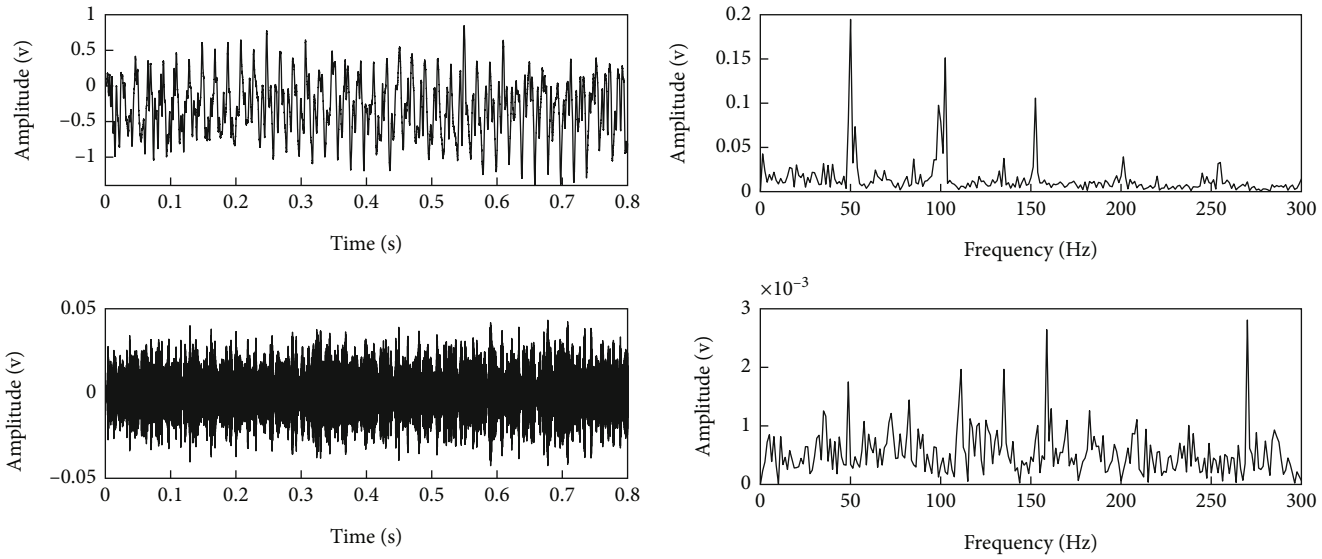

(a) The obtained two main modes using FMD

(b) Envelope spectrum of the two main modes as shown in (a)

Figure 6: Early weak fault signal of experimental rolling element bearing handled by FMD.

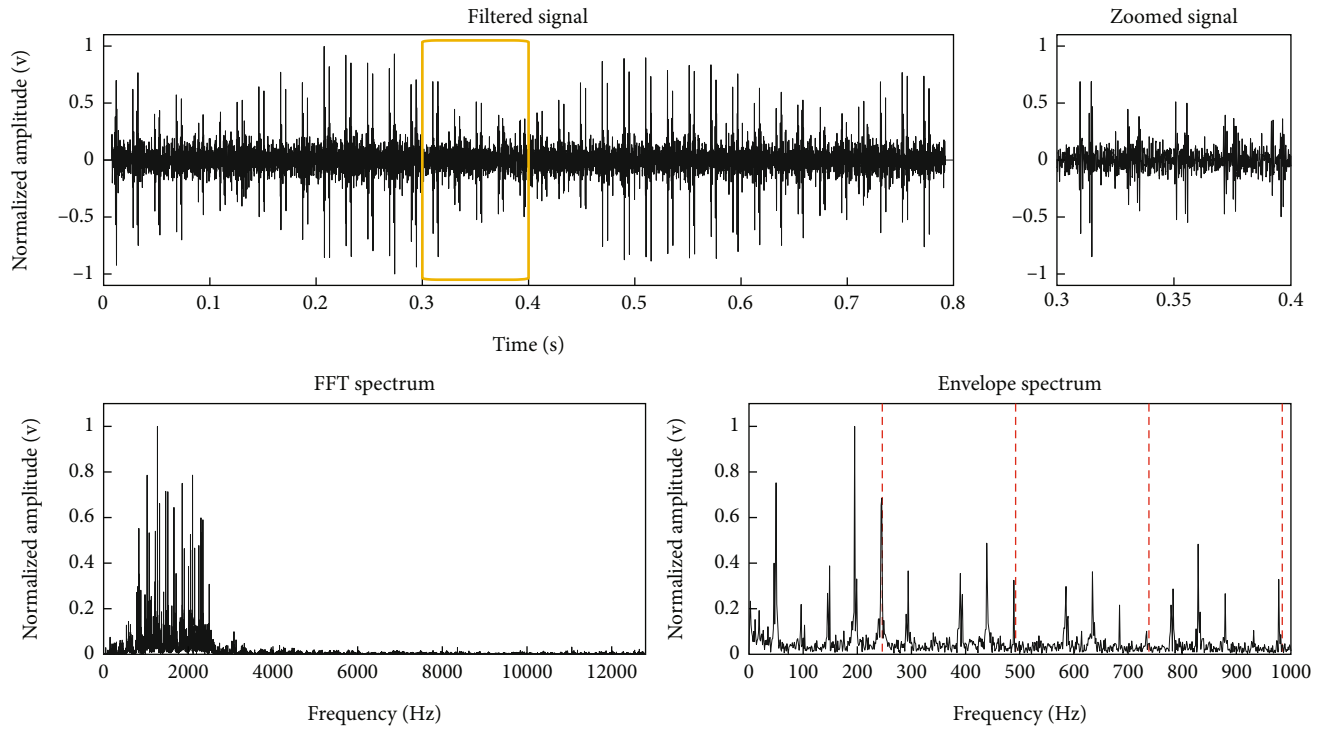

Figure 7: The proposed BD analysis result of the second mode shown in Figure 6(a).

the driving motor is decelerated by the gearbox to drive the grinding equipment to work. In the daily maintenance of the equipment, it is found that the vibration value of the free end of the motor is too large, and the measured vibration value is shown in Table 3. The free end bearing of the motor is disassembled after shutting down the equipment, and it is found that failure arises on the inner race. The real picture of the inner race fault is shown in Figure 8(b). The equipment detection instrument is the equipment status detection and safety evaluation system produced by Zhengzhou Expert Technology Co., Ltd. The sensor model is EAJ03-100, and its sensitivity is 100 mv/g. The sampling frequency and sampling length are 3200 Hz and 8192 points, respectively. The type of the monitored bearing is NU244. According to the calculation formula of the fault characteristic frequency of rolling bearing components, the calculated fault characteristic fault frequencies of the monitored bearing are shown in Table 4.

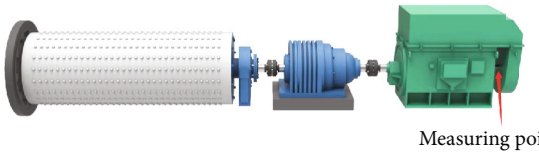

(a) Structure diagram of cement raw mill

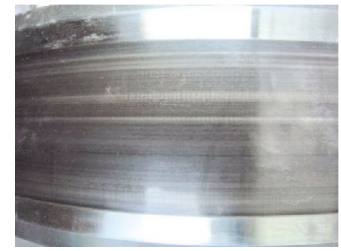

(b) Failure on the inner race of monitored engineering bearing

Figure 8: Structure of the engineering equipment and the failure on the monitored rolling bearing.

Table 3: The measured values of the measuring point.

Number	Measured point	Direction	Value (mm/s^2)	Value (mm/s)
1	Free end of motor	Horizontal	46.65	0.74
2		Vertical	26.51	0.56

Table 4: The fault characteristic frequencies of the monitored rolling element bearing.

Type	Inner race (Hz)	Outer race (Hz)	Ball (Hz)	Cage (Hz)
NU244	126.12	98.00	90.50	5.16

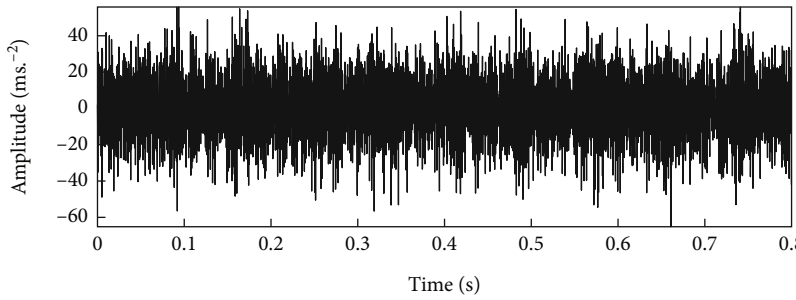

(a) Time-domain waveform of the measured signal corresponding to horizontal direction

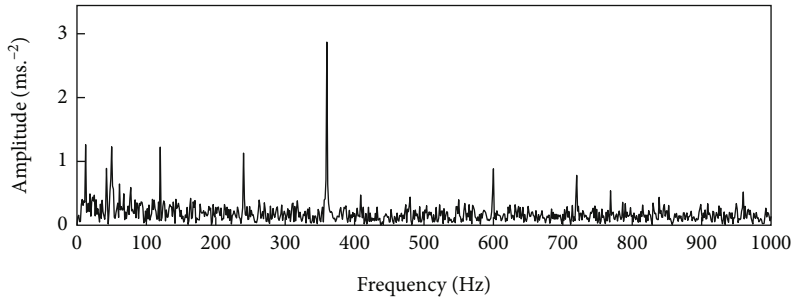

(b) Envelope spectrum of the signal as shown in (a)

Figure 9: The measured signal of the engineering bearing with its envelope spectrum result.

Effectiveness of the proposed method is verified by the vibration data of the channel with larger amplitude in Table 1, that is, the channel in the horizontal direction. Time-domain waveform and full-band ES analysis results of the analyzed data are shown in Figures 9(a) and 9(b), respectively. In Figure 9(a), although the shock features can be observed, they are not obvious enough by calculating the interval between two shocks directly, that is, the failure period. In Figure 9(b), the frequency with the larger amplitude cannot correspond to the fault characteristic frequency shown in Table 2, which can easily lead to misdiagnosis or missed diagnosis. The signal shown in Figure 9(a) is decomposed by FMD firstly according to the proposed method. The number of FMD decomposition modes is set to 4, and the corresponding decomposition results are shown in Figure 10: Figure 10(a) is the obtained two main modes,

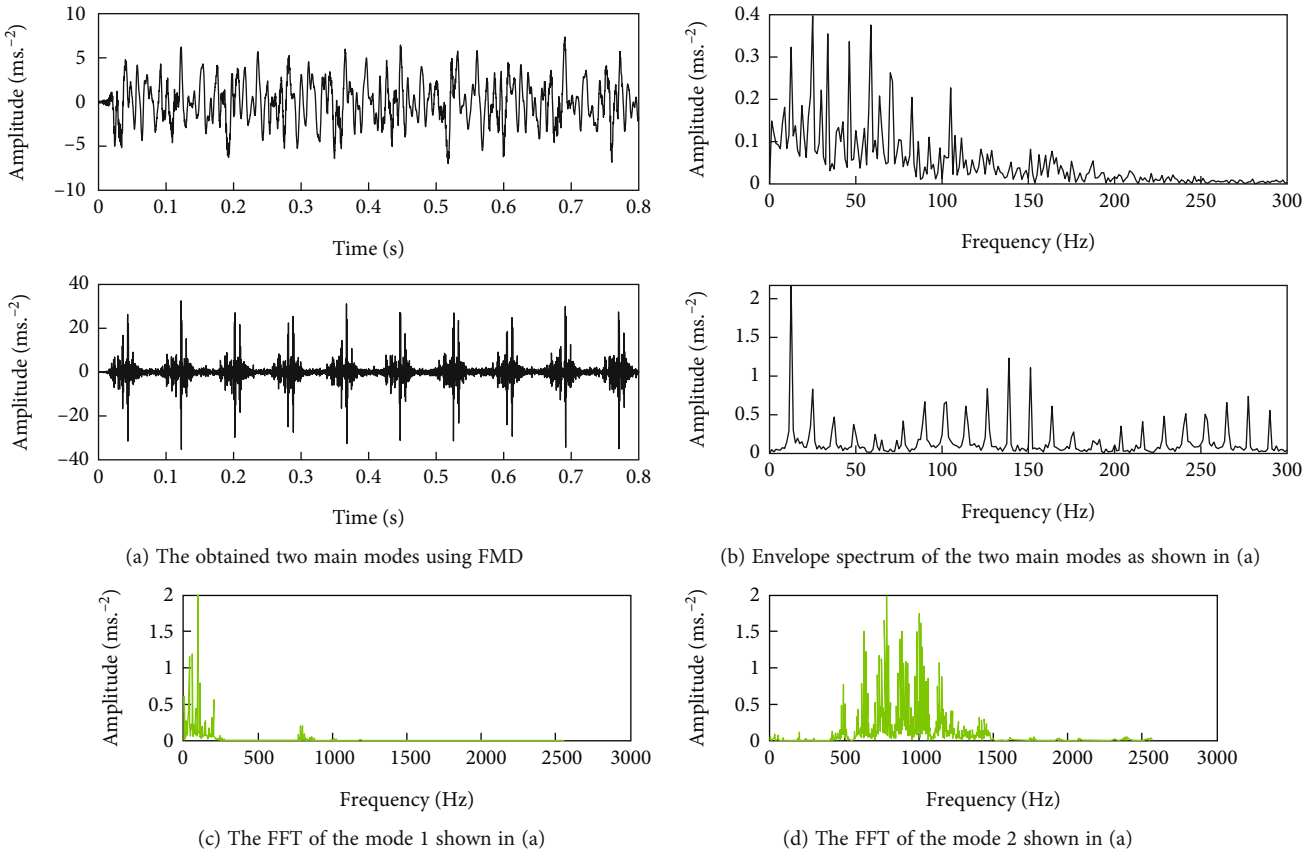

(a) The obtained two main modes using FMD

(b) Envelope spectrum of the two main modes as shown in (a)

(c) The FFT of the mode 1 shown in (a)

(d) The FFT of the mode 2 shown in (a)

Figure 10: Fault signal of engineering rolling element bearing handled by FMD.

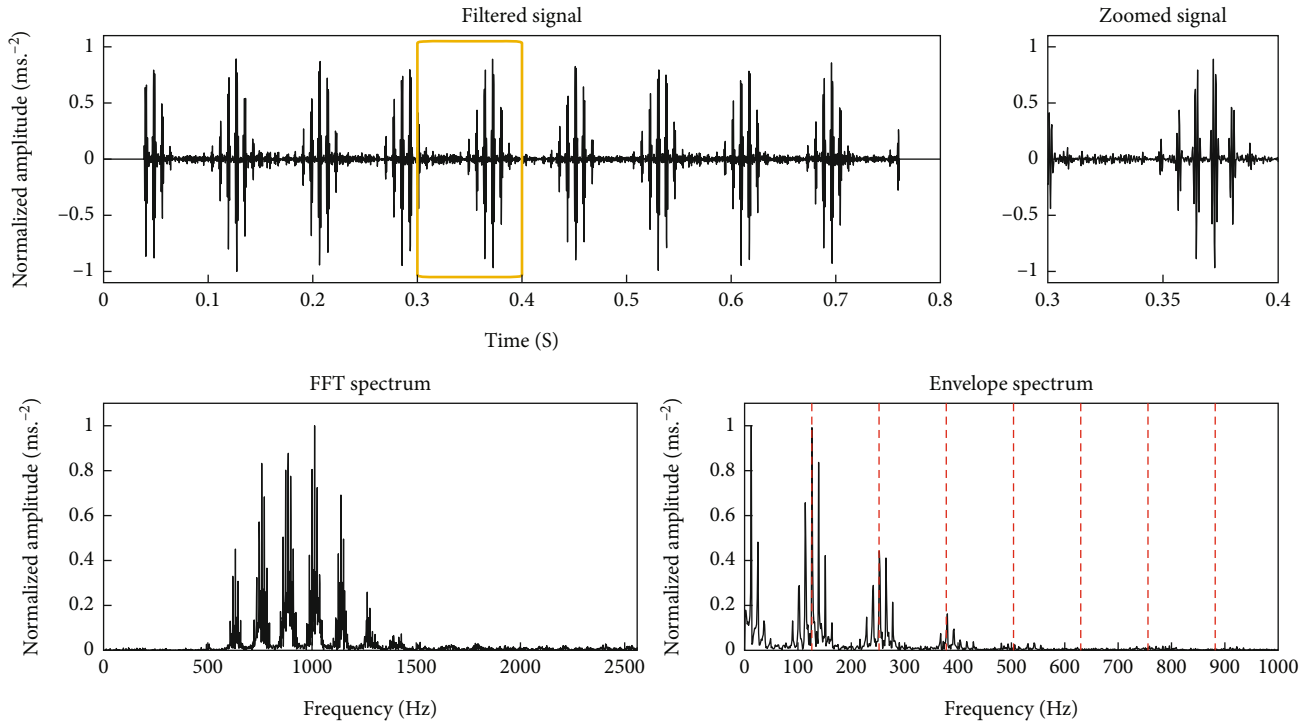

Figure 11: The proposed BD analysis result of the second mode shown in Figure 10(a).

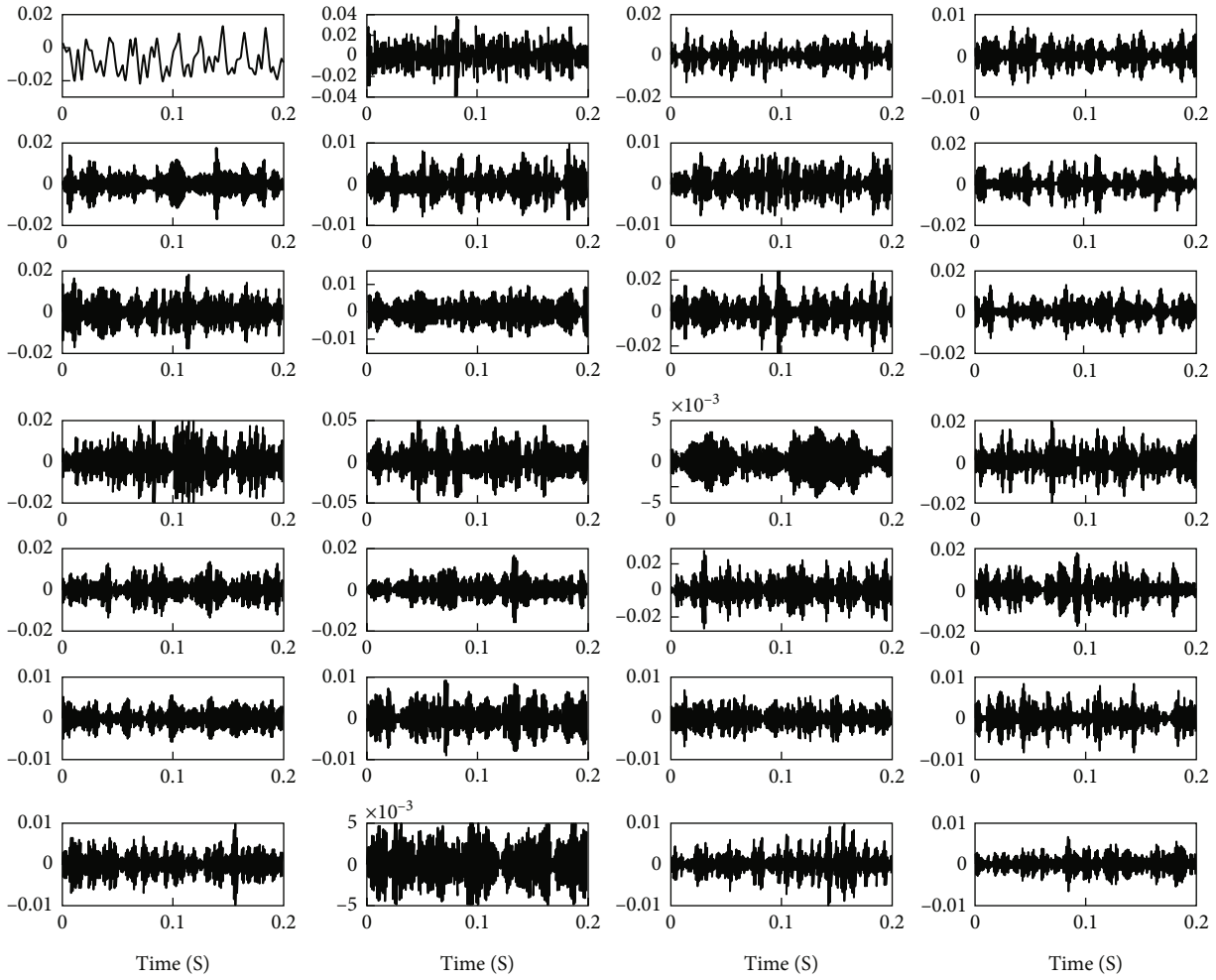

(a) Decomposition results of the signal as shown in Figure 4(c) by using SVMD

(b) The selected mode with the biggest SI

(c) Envelope spectral of the signal as shown in (b)

Figure 12: The reconstructed signal of test bearing with its envelope spectral analysis result.

and Figure 10(b) is their corresponding envelope spectrums. According to the spectral structure characteristics of Figure 10(b), FMD successfully decomposes the signal shown in Figure 9(a) into two main modes with relatively single components: The spectral line structure in the upper graph in Figure 10(b) is dominated by the rotating frequency and its harmonics, indicating that the components contained in the corresponding mode are mainly the components of motor rotating frequency signal; the fault characteristic frequency of inner race of the monitored bearing could be reflected clearly relatively in the lower graph of Figure 10(b), indicating that the corresponding mode mainly contains periodic impact characteristic components. Figures 10(c) and 10(d) are the frequency spectrum of the signals shown in Figure 10(a), which further verifies the better separation effect of the FMD method for the signal shown in Figure 9(a): The two modal signals are concentrated in the low frequency (rotation frequency and its harmonic frequency) and the high frequency part (the characteristic component of impact failure of rolling bearing). Besides, the SIs of the two modes are very

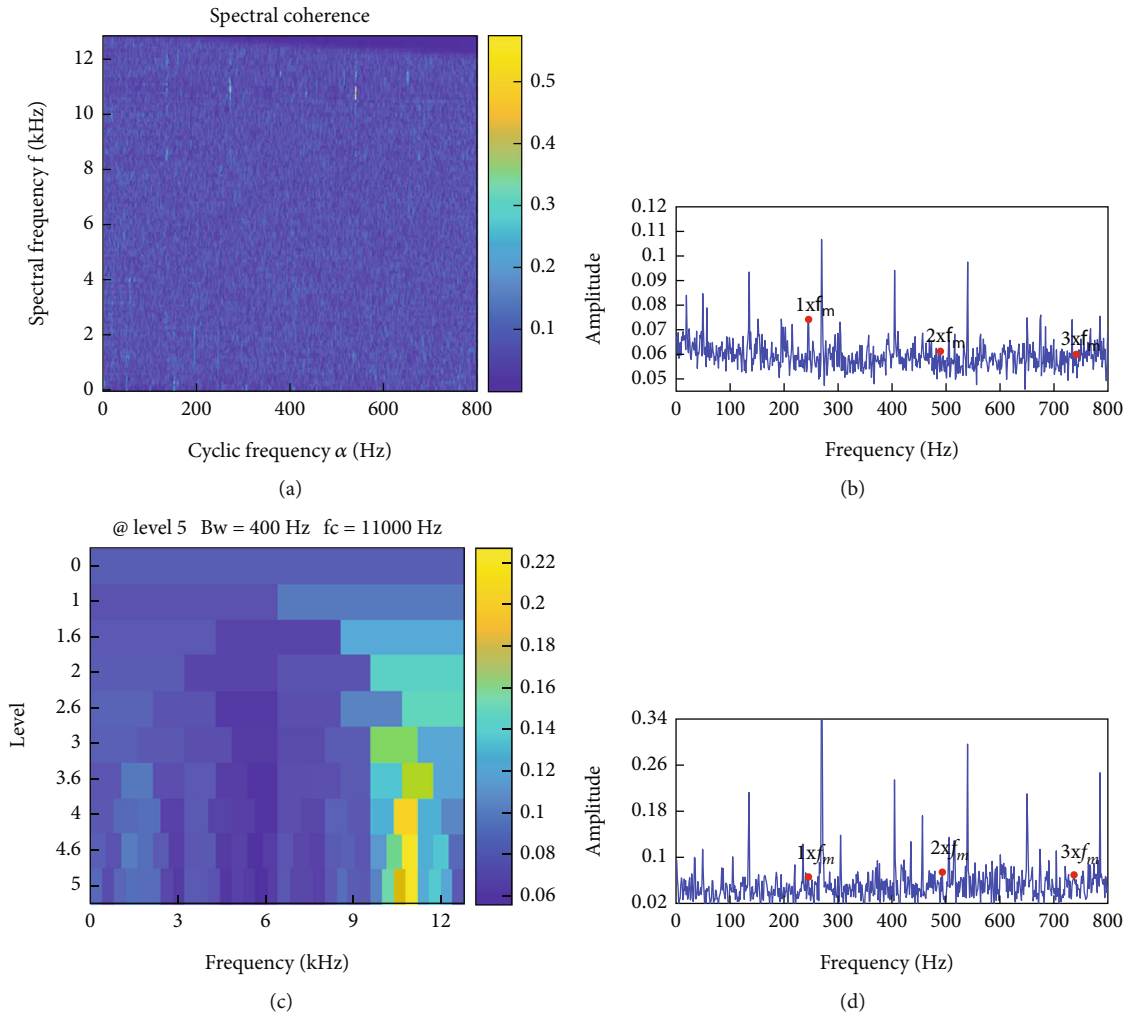

Figure 13: Analysis result of the experimental signal as shown in Figure 4(c) using IESCFFOgram.

different, and the second mode is bigger than the first mode, so the second mode is selected for further analysis. However, the motor rotating frequency and its harmonics still cause relatively strong interference on the inner race fault characteristic frequency in the lower graph of Figure 10(b). Besides, the harmonics of the inner race fault characteristic frequency are not extracted. Further fault information sensitive frequency band selection analysis is needed. Apply the BD method on the second mode as shown in Figure 10(a), and the corresponding results are given in Figure 11: Comparing the filtered signal with the original mode signal shown in Figure 10(a), the impulse characteristics of the former are not only enhanced effectively, but also, the modulation features are more obvious. Through statistical calculation, the former is 3.2 times that of the latter. Besides, it could be observed that not only the inner race fault characteristic frequency and its harmonics are extracted based on the frequency spectrum and envelope spectrum of the filtered signal but also the modulating frequency; that is, the rotating frequency is extracted when failure arises on the inner race of bearing. Effectiveness of the proposed method is further verified through the analysis results of this engineering signal.

6. Comparison

In the section, two methods are used for comparison to verify the advantages of the proposed method. The first one is a new time-frequency decomposition method, and the second one is a new frequency band selection method based on cyclostationarity.

As a relative time-frequency analysis method, successive variational mode decomposition (SVMD) [48] is an improved method of VMD, which overcomes the defect of VMD needing determine the precise number of modes in advance. Besides, the modes containing single component could be extracted successively by SVMD without needing to know the number of modes. In the section, SVMD is used to compare first and to decompose the original experimental signal shown in Figure 4(c), and the obtained series of modes are presented in Figure 12(a). Then, the SIs of the obtained modes are calculated, and the mode as shown in Figure 12(b) owning the biggest SI is selected for ES analysis, and the last result is given in Figure 12(c). The inner race fault characteristic frequency could be extracted based on Figure 12(c). However, its harmonics are not extracted the

same as the extracted result as shown in the last figure of Figure 7 by using the proposed method.

Cyclostationarity is another classical and effective method, and spectral correlation (SC) with its normalized version based on cyclostationarity, that is, SCoh [49], is the most effective second-order cyclostationary method for fault feature extraction of REB. Then, squared envelope spectrum (SES) or enhanced envelope spectrum (EES) for identifying the fault characteristic frequencies could be obtained by integrating SCoh over the whole spectral frequency band. But the defect of SES or EES is sensitive to noise. To address this issue, a feature-adaptive method called IES via Candidate Fault Frequency Optimization-gram (IESCFFOgram) [50] is proposed to determine the informative spectral frequency band from SCoh for bearing fault diagnosis, which is used as the second method for comparison. The last analysis results are given in Figure 13(d): Figure 13(a) is the spectral coherence of the signal shown in Figure 4(c), Figure 13(b) is the EES result based on Figure 13(a), and Figure 13(c) is the IESCFFOgram spectral result. Unfortunately, the inner race fault characteristic frequency is not extracted, and the main reason is due to the inference of strong background noise and the complex multicomponent of the original fault signal.

7. Conclusion

In conclusion, a two-step method by combining FMD with a BD algorithm is proposed for weak fault feature extraction of REB. Firstly, FMD taking the impulsiveness and periodicity of fault signal into consideration simultaneously is used to decompose the original complex multicomponent signal into several modes containing relative single component. Subsequently, a SI with high reliability measuring the impact characteristics is used to calculate the SIs of the obtained modes, and the mode with the largest SI is selected for further analysis. Then, the selected mode is input into the BD calculation model to further enhance the impact characteristics and remove inference of background noise. At last, apply ES on the filtered signal of the BD method, and satisfactory fault features are extracted. Besides, the following conclusions can be drawn:

(1) SI could reflect the periodic impact signal much more effectively than the other related indexes through simulation verification

(2) FMD could separate the complex multicomponent signal into several modes containing relative single component through experiment and engineering verification, which could overcome the defects of traditional time-frequency analysis methods such as wavelet transform, EMD, and VMD

(3) The BD method could enhance the impact characteristics of REB's vibration signal effectively through experiment and engineering verification

(4) The proposed combined method could extract the fault features of REB much more effective than the other methods through comparison

In addition, some parameters used in the used methods are obtained through experience and trials. So, research on adjusting the algorithm parameters will be carried out in the further work. Besides, the paper mainly solves the difficult problem of extraction of weak fault features of rolling element bearing under constant speed. In the future research, the order tracking analysis method being suitable for analyzing variable speed conditions will be combined with the proposed method to extend the research for fault diagnosis of rotating machinery working on variable speed condition and make the proposed method more universal in engineering application.

Data Availability

The data could be available on request.

Conflicts of Interest

The authors declared no potential conflicts of interest with respect to the research, authorship, and/or publication of this article.

Acknowledgments

The research is supported by the National Key R&D Program of China (approved grant: 2020YFB2007200) and the Key Science and Technology Research Project of the Henan Province (approved grant: 232102221039).

References

[1] Q. Ni, J. C. Ji, and K. Feng, "Data-driven prognostic scheme for bearings based on a novel health indicator and gated recurrent unit network," *IEEE Transactions on Industrial Informatics*, vol. 19, no. 2, pp. 1301–1311, 2023.

[2] V. K. Rai and A. R. Mohanty, "Bearing fault diagnosis using FFT of intrinsic mode functions in Hilbert-Huang transform," *Mechanical Systems and Signal Processing*, vol. 21, no. 6, pp. 2607–2615, 2007.

[3] Y. Yang, D. J. Yu, and J. S. Cheng, "A fault diagnosis approach for roller bearing based on IMF envelope spectrum and SVM," *Measurement*, vol. 40, no. 9-10, pp. 943–950, 2007.

[4] R. Zhou, W. Bao, N. Li, X. Huang, and D. Yu, "Mechanical equipment fault diagnosis based on redundant second generation wavelet packet transform," *Digital Signal Processing*, vol. 20, no. 1, pp. 276–288, 2010.

[5] J. D. Wu and Y. J. Tsai, "Speaker identification system using empirical mode decomposition and an artificial neural network," *Expert Systems with Applications*, vol. 38, no. 5, pp. 6112–6117, 2011.

[6] V. Sharma and A. Parey, "Extraction of weak fault transients using variational mode decomposition for fault diagnosis of gearbox under varying speed," *Engineering Failure Analysis*, vol. 107, article 104204, 2020.

[7] J. Antoni and R. B. Randall, "The spectral kurtosis: application to the vibratory surveillance and diagnostics of rotating

machines," *Mechanical Systems and Signal Processing*, vol. 20, no. 2, pp. 308–331, 2006.

[8] H. Y. Liu, W. G. Huang, S. B. Wang, and Z. Zhu, "Adaptive spectral kurtosis filtering based on Morlet wavelet and its application for signal transients detection," *Signal Processing*, vol. 96, pp. 118–124, 2014.

[9] D. Wang, "Some further thoughts about spectral kurtosis, spectral *L2* / *L1* norm, spectral smoothness index and spectral Gini index for characterizing repetitive transients," *Mechanical sytems and signal processing*, vol. 108, pp. 360–368, 2018.

[10] K. Zhang, P. Chen, M. R. Yang, L. Song, and Y. Xu, "The Harmogram: a periodic impulses detection method and its application in bearing fault diagnosis," *Mechanical Systems and Signal Processing*, vol. 165, article 108374, 2022.

[11] B. Zhang, Y. Miao, J. Lin, and Y. Yi, "Adaptive maximum second-order cyclostationarity blind deconvolution and its application for locomotive bearing fault diagnosis," *Mechanical Systems and Signal Processing*, vol. 158, article 107736, 2021.

[12] H. Endo and R. B. Randall, "Enhancement of autoregressive model based gear tooth fault detection technique by the use of minimum entropy deconvolution filter," *Mechanical Systems and Signal Processing*, vol. 21, no. 2, pp. 906–919, 2007.

[13] G. L. McDonald, Q. Zhao, and M. J. Zuo, "Maximum correlated kurtosis deconvolution and application on gear tooth chip fault detection," *Mechanical Systems and Signal Processing*, vol. 33, pp. 237–255, 2012.

[14] R. K. Duan, Y. H. Liao, L. Yang, J. Xue, and M. Tang, "Minimum entropy morphological deconvolution and its application in bearing fault diagnosis," *Measurement*, vol. 182, article 109649, 2021.

[15] Y. Cheng, N. Zhou, W. H. Zhang, and Z. Wang, "Application of an improved minimum entropy deconvolution method for railway rolling element bearing fault diagnosis," *Journal of Sound and Vibration*, vol. 425, pp. 53–69, 2018.

[16] Z. Wang, J. Zhou, W. Du, Y. Lei, and J. Wang, "Bearing fault diagnosis method based on adaptive maximum cyclostationarity blind deconvolution," *Mechanical Systems and Signal Processing*, vol. 162, article 108018, 2022.

[17] A. Napolitano, "Cyclostationarity: limits and generalizations," *Signal Processing*, vol. 120, pp. 323–347, 2016.

[18] A. I. R. Fontes, J. B. A. Rego, A. D. Martins, L. F. Q. Silveira, and J. C. Principe, "Cyclostationary correntropy: definition and applications," *Expert Systems with Application*, vol. 69, pp. 110–117, 2017.

[19] K. Feng, W. A. Smith, P. Borghesani, R. B. Randall, and Z. Peng, "Use of cyclostationary properties of vibration signals to identify gear wear mechanisms and track wear evolution," *Mechanical Systems and Signal Processing*, vol. 150, article 107285, 2021.

[20] B. K. Yan, B. Wang, F. X. Zhou, W. Li, and B. Xu, "Sparse decomposition method based on time-frequency spectrum segmentation for fault signals in rotating machinery," *ISA Transactions*, vol. 83, pp. 142–153, 2018.

[21] Q. C. Li, X. X. Ding, W. B. Huang, Q. He, and Y. Shao, "Transient feature self-enhancement via shift-invariant manifold sparse learning for rolling bearing health diagnosis," *Measurement*, vol. 148, article 106957, 2019.

[22] J. M. Li, X. F. Yao, H. Wang, and J. Zhang, "Periodic impulses extraction based on improved adaptive VMD and sparse code shrinkage denoising and its application in rotating machinery fault diagnosis," *Mechanical Systems and Signal Processing*, vol. 126, pp. 568–589, 2019.

[23] Y. Kong, T. Y. Wang, Z. P. Feng, and F. Chu, "Discriminative dictionary learning based sparse representation classification for intelligent fault identification of planet bearings in wind turbine," *Renewable Energy*, vol. 152, pp. 754–769, 2020.

[24] T. Han, D. X. Jiang, Y. K. Sun, N. Wang, and Y. Yang, "Intelligent fault diagnosis method for rotating machinery via dictionary learning and sparse representation-based classification," *IEEE Transactions on Industrial Informatics*, vol. 118, pp. 181–193, 2018.

[25] K. Zhang, W. M. Zuo, Y. J. Chen, D. Meng, and L. Zhang, "Beyond a Gaussian denoiser: residual learning of deep CNN for image denoising," *IEEE Transactions on Image Processing*, vol. 26, no. 7, pp. 3142–3155, 2017.

[26] X. C. Liu, Q. C. Zhou, J. Zhao, H. Shen, and X. Xiong, "Fault diagnosis of rotating machinery under noisy environment conditions based on a 1-D convolutional autoencoder and 1-D convolutional neural network," *Sensors*, vol. 19, no. 4, p. 972, 2019.

[27] H. M. Shi, J. C. Chen, J. Si, and C. Zheng, "Fault diagnosis of rolling bearings based on a residual dilated pyramid network and full convolutional denoising autoencoder," *Sensors*, vol. 20, no. 20, p. 5734, 2020.

[28] G. Fan, J. Li, and H. Hao, "Vibration signal denoising for structural health monitoring by residual convolutional neural networks," *Measurement*, vol. 157, article 107651, 2020.

[29] J. B. Yu and X. K. Zhou, "One-dimensional residual convolutional autoencoder based feature learning for gearbox fault diagnosis," *IEEE Transactions on Industrial Informatics*, vol. 16, no. 10, pp. 6347–6358, 2020.

[30] H. Han, H. Wang, Z. Liu, and J. Wang, "Intelligent vibration signal denoising method based on non-local fully convolutional neural network for rolling bearings," *ISA Transactions*, vol. 122, pp. 13–23, 2022.

[31] J. M. Li, Q. W. Yu, X. D. Wang, and Y. Zhang, "An enhanced rolling bearing fault detection method combining sparse code shrinkage denoising with fast spectral correlation," *ISA Transactions*, vol. 102, pp. 335–346, 2020.

[32] C. Cabrelli, "Minimum entropy deconvolution and simplicity: a noniterative algorithm," *Geophysics*, vol. 50, no. 3, pp. 394–413, 1985.

[33] Y. Cheng, Z. Wang, W. Zhang, and G. Huang, "Particle swarm optimization algorithm to solve the deconvolution problem for rolling element bearing fault diagnosis," *ISA Transactions*, vol. 90, pp. 244–267, 2019.

[34] Y. H. Miao, J. J. Wang, B. Y. Zhang, and H. Li, "Practical framework of Gini index in the application of machinery fault feature extraction," *Mechanical Systems and Signal Processing*, vol. 165, article 108333, 2022.

[35] D. Zonoobi, A. A. Kassim, and Y. V. Venkatesh, "Gini index as sparsity measure for signal reconstruction from compressive samples," *IEEE Journal on Selected Topics in Signal Processing*, vol. 5, no. 5, pp. 927–932, 2011.

[36] X. Jia, M. Zhao, Y. Di, P. Li, and J. Lee, "Sparse filtering with the generalized l_p/l_q norm and its applications to the condition monitoring of rotating machinery," *Mechanical Systems and Signal Processing*, vol. 102, pp. 198–213, 2018.

[37] L. Li, "Sparsity-promoted blind deconvolution of ground-penetrating radar (GPR) data," *IEEE Geoscience and Remote Sensing Letters*, vol. 11, no. 8, pp. 1330–1334, 2014.

[38] G. L. McDonald and Q. Zhao, "Multipoint optimal minimum entropy deconvolution and convolution fix: application to vibration fault detection," *Mechanical Systems and Signal Processing*, vol. 82, pp. 461–477, 2017.

[39] X. Zhang, S. T. Wan, Y. L. He, X. Wang, and L. Dou, "Teager energy spectral kurtosis of wavelet packet transform and its application in locating the sound source of fault bearing of belt conveyor," *Measurement*, vol. 173, article 108367, 2021.

[40] M. Buzzoni, J. Antoni, and G. D'Elia, "Blind deconvolution based on cyclostationarity maximization and its application to fault identification," *Journal of Sound and Vibration*, vol. 432, pp. 569–601, 2018.

[41] T. Guo and Z. M. Deng, "An improved EMD method based on the multi-objective optimization and its application to fault feature extraction of rolling bearing," *Applied Acoustics*, vol. 127, pp. 46–62, 2017.

[42] J. Wang, G. Du, Z. Zhu, C. Shen, and Q. He, "Fault diagnosis of rotating machines based on the EMD manifold," *Mechanical Systems and Signal Processing*, vol. 135, article 106443, 2020.

[43] C. Yin, Y. L. Wang, G. C. Ma, Y. Wang, Y. Sun, and Y. He, "Weak fault feature extraction of rolling bearings based on improved ensemble noise-reconstructed EMD and adaptive threshold denoising," *Mechanical Systems and Signal Processing*, vol. 171, article 108834, 2022.

[44] Y. H. Miao, B. Y. Zhang, C. H. Li, J. Lin, and D. Zhang, "Feature mode decomposition: new decomposition theory for rotating machinery fault diagnosis," *IEEE Transactions on Industrial Electronics*, vol. 70, no. 2, pp. 1949–1960, 2023.

[45] B. Fang, J. Hu, C. Yang, and X. M. Chen, "Minimum noise amplitude deconvolution and its application in repetitive impact detection," *Structural Health Monitoring*, vol. 22, no. 3, pp. 1807–1827, 2023.

[46] D. A. Fournier, H. J. Skaug, J. Ancheta et al., "AD model builder: using automatic differentiation for statistical inference of highly parameterized complex nonlinear models," *Optimization Methods and Software*, vol. 27, no. 2, pp. 233–249, 2012.

[47] M. Zhao, J. Lin, Y. H. Miao, and X. Xu, "Feature mining and health assessment for gearboxes using run-up/coast-down signals," *Sensors*, vol. 16, no. 11, p. 1837, 2016.

[48] N. Nazari and S. M. Sakhaei, "Successive variational mode decomposition," *Signal Processing*, vol. 174, article 107610, 2020.

[49] J. Antoni, "Cyclostationarity by examples," *Mechanical Systems and Signal Processing*, vol. 23, no. 4, pp. 987–1036, 2009.

[50] Y. Cheng, S. B. Wang, B. Y. Chen et al., "An improved envelope spectrum via candidate fault frequency optimization-gram for bearing fault diagnosis," *Journal of Sound and Vibration*, vol. 523, article 116746, 2022.